Experimental Demonstration of Directive Si_3N_4 Optical Leaky Wave Antennas With Semiconductor Perturbations

Qiancheng Zhao, *Student Member, IEEE*, Caner Guclu, *Student Member, IEEE*, Yuewang Huang, Filippo Capolino, *Senior Member, IEEE*, and Ozdal Boyraz, *Senior Member, IEEE*

***Abstract*—Directive optical leaky wave antennas (OLWAs) fabricated in CMOS-compatible semiconductor planar waveguide technology have the potential to provide high directivity with electrical tunability promising for modulation and switching capabilities. We experimentally demonstrate directive radiation from a silicon nitride (Si_3N_4) waveguide-based OLWA. The OLWA design comprises a crystalline silicon (Si) nanowire array buried inside a Si_3N_4 waveguide. Each Si nanowire has a width of 260 nm and a height of 150 nm. The OLWA is designed to exhibit a directive radiation pattern at telecom wavelengths. The measured radiation pattern at the wavelength 1550 nm has its maximum emission intensity at the angle of 85.1° relative to the waveguide axis and a half-power beam width of approximately 5.0°, which are consistent with our theoretical predictions. The results indicate that the TM mode is more radiative than the TE mode in our fabricated devices. Also, the radiation pattern of the measured OLWA shows dependence on wavelength, which is typical of leaky wave antennas. The device is promising in chip-to-space optical interconnect applications.**

***Index Terms*—Directive antennas, gratings, leaky wave antennas, optical antennas, silicon nitride.**

I. Introduction

LEAKY wave antennas are a class of antennas that use travelling waves to produce narrow radiated beams [1]. The theory and applications of leaky waves (LWs) have been extensively developed since the first known LW antenna introduced by W.W. Hansen in 1940 [2]. A fundamental method of achieving LW radiation is to use waveguides with periodic features, which consists of a waveguide supporting a slow (guided) wave that has been periodically modulated along the waveguide axis. The periodic modulations create an infinite number of Floquet harmonics, among which one Floquet harmonic will be a fast wave and thus can be leaked as a radiating wave [3], [4]. The LW antennas have the advantage of radiating in either forward or backward directions, as its beam will scan a range of angles by changing frequency. Many LW antennas, including corrugated metal films [5]–[9] and plasmonic nanosphere arrays [10]–[12], utilize periodic structures to enhance radiation in optical frequencies. Besides metallic structures, dielectric-based periodic antennas have also been widely used in millimeter wave [13] and optical applications [14].

Optical leaky wave antennas (OLWAs) can direct light, focus energy, and enhance light-matter interaction. Therefore, they are promising for applications such as free space optical communications [15], space-division multiplexing [16], [17], and tunable grating couplers [18], [19]. We have recently introduced the theory of CMOS compatible OLWAs [20]–[22] that provides directive radiation at 1550 nm in a dielectric waveguide comprising periodic semiconductor perturbations. Readers may refer to our previous work [20]–[24] for further information on the theoretical design and preliminary investigations on its modulation capability. The device is designed on a silicon nitride (Si_3N_4) on silicon-on-insulator (SOI) platform that has drawn tremendous interest as a promising solution to integrated optical interconnections in recent years [25]–[27]. Silicon nitride is chosen as the dielectric waveguide material due to its low propagation loss, wide transparent window and silicon-compatible fabrication technology [28]. The SOI platform, which reached a mature stage for integrated silicon photonics, is chosen to build the silicon nanowires. SOI has been widely used to deliver chip-scale passive photonic devices, imaging devices [29], and nonlinear devices [30] with CMOS fabrication compatibility [31]. The aforementioned very slowly attenuating LW is realized by designing the silicon nanowires buried inside the Si_3N_4 waveguide with a small filing factor. The electrical control capability of the proposed OLWA can be achieved by engineering the optical parameters of Si via plasma dispersion effect [32], [33] or Franz-Keldysh effect [34].

In this paper, we present the experimental demonstration of a CMOS-compatible OLWA made of a dielectric waveguide and semiconductor perturbations. The OLWA radiation pattern is characterized in the altitude angle θ ranging from 65° to 112° with a radiation peak occurring at 85.1° and a half-power beam width of 5.0° at 1550 nm wavelength. The main beam is well resolved in the experiments together with the frequency-dependent far-field scanning. All side lobes are at least 7 dB below the main lobe, indicating a directive emission. This is the first demonstration of embedding silicon wires as perturbations in a dielectric waveguide in a CMOS compatible fabrication manner. The incorporation of semiconductor enables electrical

Manuscript received June 1, 2016; accepted September 9, 2016. Date of publication September 12, 2016; date of current version October 13, 2016. This work was supported in part by the National Science Foundation under NSF Award # ECCS-1028727 and NSF Award # ECCS-1449397.

Q. Zhao, C. Guclu, F. Capolino, and O. Boyraz are with the Department of Electrical engineering and Computer Science, University of California, Irvine, CA 92697 USA (e-mail: qianchez@uci.edu; cguclu@uci.edu; f.capolino@uci.edu; oboyraz@uci.edu).

Y. Huang was with the Department of Electrical engineering and Computer Science, University of California, Irvine, CA 92697 USA. He is now with Apple Inc., Cupertino, CA 95014 USA (e-mail: yuewangh@uci.edu).

Color versions of one or more of the figures in this paper are available online at http://ieeexplore.ieee.org.

Digital Object Identifier 10.1109/JLT.2016.2608801

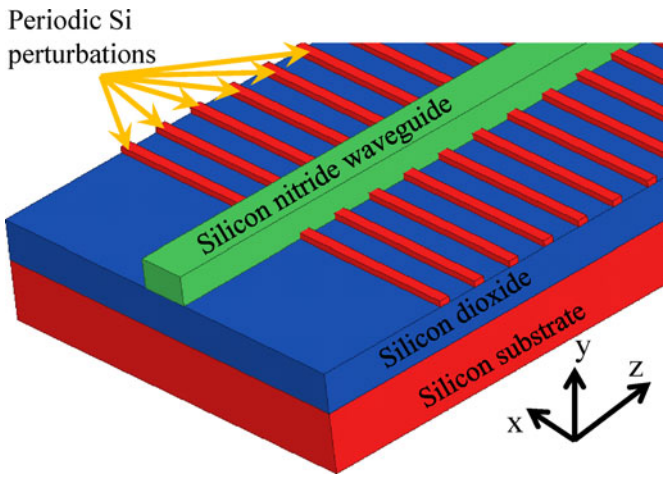

Fig. 1. Schematic of the OLWA made of a Si_3N_4 waveguide over the periodic Si perturbations for possible electronic control.

control on the radiation, which can be utilized in chip-to-space communications [35].

This paper is organized as follows. Section II briefly introduces the LW principles. Section III includes the OLWA fabrication procedure, experiment setup, and testing results. The radiation pattern is examined to reveal its wavelength-dependence and polarization-dependence. A numerical simulation is also included for verification. In Section IV, we summarize the performance of the OLWA and discuss its potential applications.

II. Theoretical Analysis

The geometry of the radiating structure under study is shown in Fig. 1. The OLWA consists of a Si_3N_4 waveguide with buried Si perturbations on an SOI platform. The slow wave guided by the Si_3N_4 waveguide becomes leaky due to the periodic Si perturbations. The overall leaky mode that propagates in the waveguide can be represented as a superposition of an infinite set of Floquet spatial harmonics travelling with wave numbers $k_{z,n} = \beta_{z,n} + i\alpha_z$ [22], where $\beta_{z,n} = \beta_{z,0} + 2\pi n/d$ and z is assumed to be the direction of propagation. Here, n is an integer from -∞ to +∞ that tags the n-th spatial harmonic, $\beta_{z,0}$ is the fundamental harmonic's phase constant, and d is the period of the perturbations. All spatial harmonics have the same attenuation constant α_z [9], [20], [22] among which, one of them is engineered to be a fast wave that leads to the LW radiation. Usually this fast harmonic is the $n = -1$ harmonic, and thus $\beta_{z,-1} = \beta_{z,0} - 2\pi/d$ such that $|\beta_{z,-1}| < k_h$, with k_h the wavenumber in the host medium. The leaky harmonic's electric field propagates as

$$\mathbf{E}(x,y,z) = \mathbf{E}_{-1}(x,y)\, e^{i\beta_{z,-1}z} e^{-\alpha_z z} \tag{1}$$

along the perturbed section of the waveguide. It is important to stress that the leaky wave is not bounded to the waveguide. On a radiation aperture chosen sufficiently above and outside the waveguide, the field can be assumed as only composed of –1 harmonic, since all other harmonics have their field distributions strictly confined in the waveguide core.

The radiated beam from such an antenna can be modeled by using equivalent aperture integration technique, in which most of the radiation is directed to $\theta = \theta_0$ where θ_0 is determined by the expression $\cos\theta_0 = \beta_{z,-1}/k_h$ [20]. We have used the information that the radiated beam is generated by the –1 harmonic. Therefore, the radiation close to the "broadside" direction (e.g., the direction almost orthogonal to the waveguide axis z) is obtained when $\beta_{z,-1} \ll k_h$. Values for the actual LW antenna studied in this paper are given in Appendix. The normalized far-field pattern on the y-z plane is derived as [20],

$$F(\theta) = \left| \frac{\sin\left[\left(k_h \cos\theta - k_{z,-1}\right)\frac{L}{2}\right]}{\left(k_h \cos\theta - k_{z,-1}\right)\frac{L}{2}} \right| \tag{2}$$

where L is the length of the radiating aperture assumed equal to the length of the OLWA. The leaky harmonic's wave number $k_{z,-1}$ can be extracted from the full-wave simulations by sampling the field periodically along the perturbed waveguide, and then the phase constant and the attenuation constant can be recovered by fitting curves to the simulated field's phase and amplitude profile as shown in Ref. [20]. We stress that the waveguide has two fundamental modes called TM and TE modes which are respectively defined as (i) the vertically electric field polarized mode which has perfect magnetic conductor symmetry with respect to the y-z plane and (ii) the horizontally electric field polarized mode which has perfect electric conductor symmetry with respect to y-z plane. When the waveguide is periodically perturbed, both of these modes may lead to leaky-wave radiation whose far-field pattern can be approximated by Eq. (2). It is elaborated in the following section that only the TM mode radiation is observable in the conducted experiment.

III. Experimental Results

A. OLWA Fabrication

The OLWA is fabricated on an SOI wafer [36] with 1 μm thick silicon dioxide (SiO_2) buffer layer. The Si device layer, in which the nanowires are patterned, is thinned to be 150 nm thick by dry etching and coated with back anti-reflection coating (BARC) layer and the photoresist. Lithography is implemented via an ASML 5500 optical stepper, followed by fluorine RIE plasma etching to transfer patterns from the photoresist to the Si device layer. The fabricated Si nanowires are shown in Fig. 2(a). The narrow vertical lines are the Si wires which are connected to a Si "skeleton" to prevent the nanowires from being peeled off. The array has 50 nanowires with a spatial periodicity $d = 1$ μm, and each wire is measured to be 260 nm wide in the z direction. The Si_3N_4 waveguides are then deposited by the low-pressure chemical vapor deposition (LPCVD) method with a stoichiometric recipe, and patterned by standard optical lithography, followed by fluorine RIE etching. The fabricated Si_3N_4 waveguide is shown in Fig. 2(b), extending horizontally in the SEM image. The waveguide that is used in our experiments is measured to be 1 μm wide (in the x direction) and 735 nm thick (in the y direction).

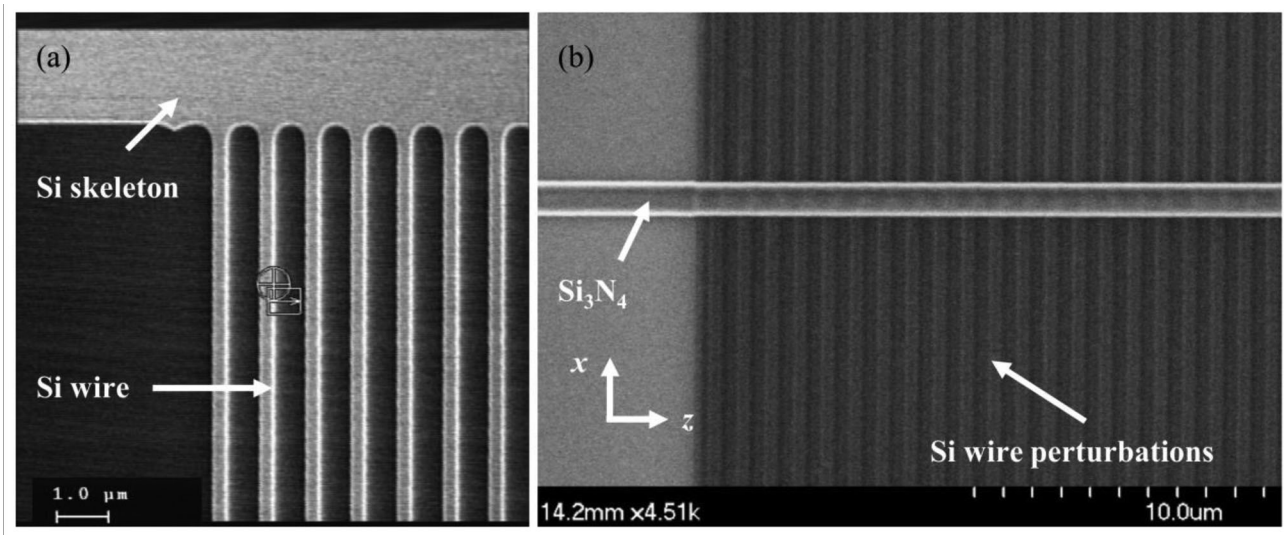

Fig. 2. (a) Scanning electron microscopy (SEM) image of the fabricated Si perturbations. (b) SEM picture of the fabricated Si_3N_4 waveguide sitting on the periodic Si perturbations.

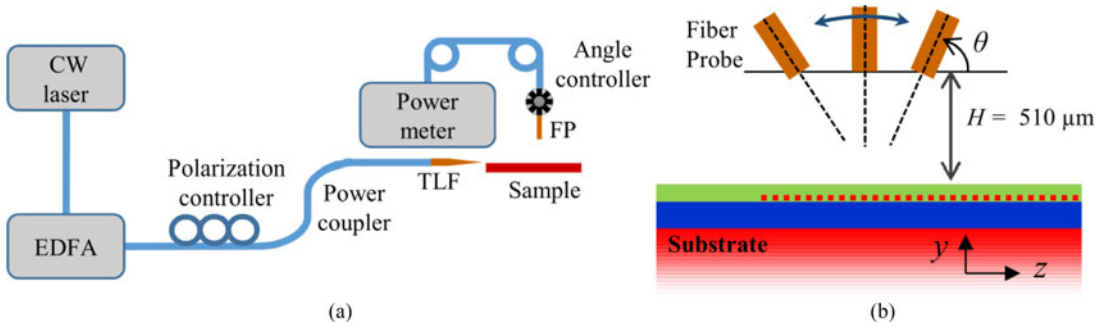

Fig. 3. (a) Schematic of the OLWA radiation pattern measurement setup. EDFA, TLF, and FP stand for erbium-doped fiber amplifier, tapered lens fiber, and fiber probe, respectively. (b) Schematic of the various FP orientations during the measurement of radiated power at various angular directions. The angle between the radiation detection direction and the waveguide propagation direction is denoted as θ.

B. Measurement Setup and Procedure

The OLWA is designed to radiate in both upward and downward directions off the wafer plane. The Si substrate bottom surface is rough and difficult to detect experimentally. Therefore, we only report the characterization of the radiation in the upward direction. The experimental setup that is utilized in the measurement of the far-field patterns is illustrated in Fig. 3(a). A tunable infrared laser (MLS-2100, Santec) is used as the source, followed by an erbium-doped fiber amplifier (EDFA, AEDFA-C-231-R, Amonics) to boost the power. To feed the antenna, a tapered and lensed fiber (TLF, OZ Optics Ltd.) is employed to butt-couple light into the waveguide facet. The polarization of the light at the TLF is handled by the polarization controller depicted in Fig. 3(a).

On the detection arm, a cleaved SM-28 fiber probe (FP) is used to detect the radiation above the OLWA device. Due to the single mode fiber's small numerical aperture, the FP has a half power beam width of approximately 3° and an antenna directivity of 26 dB. It is a directive detector and thus must be properly oriented. An angle controller is employed to adjust the FP direction. An optical power meter (1830-C, Newport Corporation) is employed to monitor the power collected by the FP.

Before we start the measurement of radiation pattern, the FP is oriented at a reference angle θ_f (e.g. $\theta_f = 85°$ that is close to the expected maximum radiation angle) and we make sure it points to the antenna by controlling its position along the z axis to maximize the power reception for that fixed FP orientation. Then the polarization controller preceding the TLF is adjusted for maximizing the reception power at the FP, and this polarization state is not altered during the radiation pattern measurement.

The radiation intensity measurement at a certain angle θ starts by first orienting the FP along θ. Next the FP is horizontally scanned along the z axis by a mechanical stage via fine tuning until the maximum power reception is achieved. In doing so, we maintain a constant vertical distance of $H = 510\ \mu$m between the FP tip to the waveguide surface as shown in Fig. 3(b). Maximum power reception occurs when the FP points to the antenna since the FP is a directive detector. This maximum power is recorded as $P_{\text{probe}}(\theta, R)$ which is the power received at angle θ and at the distance $R = H/\sin\theta$ between the FP and the OLWA radiation center. The steps above are repeated for every angle

θ reported in the radiation pattern. Since the radiation intensity scales proportionally to $1/R^2$, the radiation pattern $P(\theta)$ is then retrieved by

$$P(\theta) = R^2 P_{\text{probe}}(\theta, R) = P_{\text{probe}}(\theta, R) \frac{H^2}{\sin^2\theta} \qquad (3)$$

During the radiation pattern measurement, the reception power data are prone to temporal power drift due to the mechanical instability of the translational stages. Each angular sweep starts with $\theta = 65^\circ$ and ends with $\theta = 110^\circ$ in our experiment. In order to compensate for power drift, the power reception at $\theta = 65^\circ$ is measured twice, before and after the angular sweep. The ratio of the power measured at $\theta = 65^\circ$ after the whole angular sweep over the power measured at $\theta = 65^\circ$ before the angular sweep is denoted as η. This ratio reflects the temporal power drift of the system. To compensate the drift, the power measured at each angle is weighted by a factor between 1 and $1/\eta$ by assuming that the drift is linear with time, and assuming that the angle measurements are separated by equal time intervals. It is worth noting that the power drift did not bring the signal at the far field below the noise level. It could be removed with better controlled stages.

The FP tip in our measurement setup is not in the far-field in the strict sense, as a sacrifice to increase the dynamic range of the power reception. The OLWA length is $D = 50\,\mu$m, accordingly the far field is at a distance larger than $2D^2/\lambda_0 \approx 3225\ \mu$m and the reactive near-field boundary is at a distance larger than $0.62(D^3/\lambda_0)^{1/2} \approx 176\ \mu$m [37]. Note that the *effective* OLWA length (i.e., the length where most of the radiation comes from owing to the exponential decay. It could be defined as the effective aperture, but in one dimension) is shorter than D. However, considering the whole OLWA length D in the calculation lets us have a conservative estimation of field boundaries. The measurement distance $H = 510\ \mu$m falls into the Fresnel region, i.e., in the radiating near-field region [37], located between the reactive near field boundary and the far field boundary. In Appendix, we prove that the quasi far-field pattern collected at $H = 510\ \mu$m height is quite close to the accurate far field pattern.

C. Radiation Pattern

The measured and simulated radiation patterns on the *y-z* plane, normalized to their individual maxima, are compared in Fig. 4. The measured radiation pattern at the wavelength of 1550 nm has its maximum intensity at the angle of 85.1° and a half-power beam width of approximately 5.0°. The radiation peak angle θ_p is calculated as $\theta_p = (\theta_{-3\text{dB,left}} + \theta_{-3\text{dB,right}})/2$ to average out the noise effects, where $\theta_{-3\text{dB}}$ denotes the angle at which the radiation intensity drops to one half of its maximum. Side lobes are at least 7 dB below the dominant main lobe. Since the silicon perturbations are at the base of the waveguide, a significant part of the radiation power will go downwards into the silicon substrate but not only upward, which causes the side lobe ratio in the upward radiation direction to be limited. Note that the bottom surface is rough, therefore it diffuses downward radiation. Radiation configurations could be

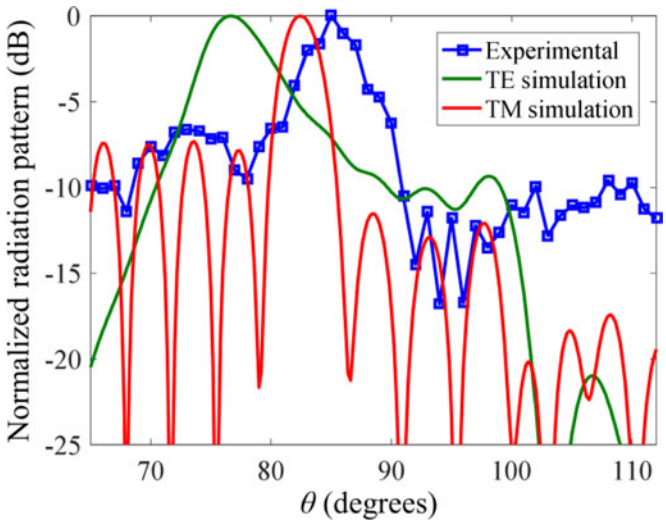

Fig. 4. Measured (blue) and simulated radiation patterns (on the *y-z* plane) generated by TE (green) and TM (red) waveguide modes at 1550 nm wavelength as a function of θ, normalized by their maximum intensities.

actually optimized to maximize the upward radiation by also including matching and reflecting layers. Experimental results are compared to the full-wave simulations using the frequency domain finite elements method (implemented in HFSS by Ansys Inc.), assuming that either the fundamental TE or TM mode is propagating in the waveguide. In the simulation model, Si, Si_3N_4 and SiO_2 relative permittivities at 1550 nm are assumed to be 12.11, 3.61, and 2.33, respectively. The far-field radiation patterns are simulated without taking into account the aperture of the FP, i.e., they provide the OLWA radiation pattern without averaging over the FP aperture. However, the averaging effect of the fiber tip may wash out the nulls and slightly broaden the main lobe's beam width in the measured pattern. Experimental results (the blue curve in Fig. 4) match the simulated radiation pattern only when a TM polarized wave (the red curve in Fig. 4) is excited in the waveguide in the simulation model. This leads to an initial guess that the TE mode excited in the waveguide does not result in a significant contribution in the measured far-field pattern, as it will be further clarified in the following text. The simulated radiation pattern has an emission peak at 82.4° with a beam width around 4.0°. Given the experimental limitations, the experimental and numerical results are in good agreement.

The observation that the simulated TM mode radiation pattern matches the experimental far-field pattern rather than the TE mode can be attributed to two different reasons (i) the TM mode radiation pattern has a simulated peak around 82.4° whereas the TE mode radiation pattern is not expected to have any sharp radiation peak around 85.1°, and (ii) the TE mode is expected to suffer heavier attenuation than the TM mode does from the TLF excitation point to the FP. We estimate that the TE mode suffers *at least* 7 dB more power loss, including the wave propagation loss and the inferior radiation gain, than the TM mode. The difference between the attenuation of the TM and TE modes is mainly caused by fabrication imperfections.

To further strengthen our explanation, we discuss next the details of a new set of measurements, aiming to find the

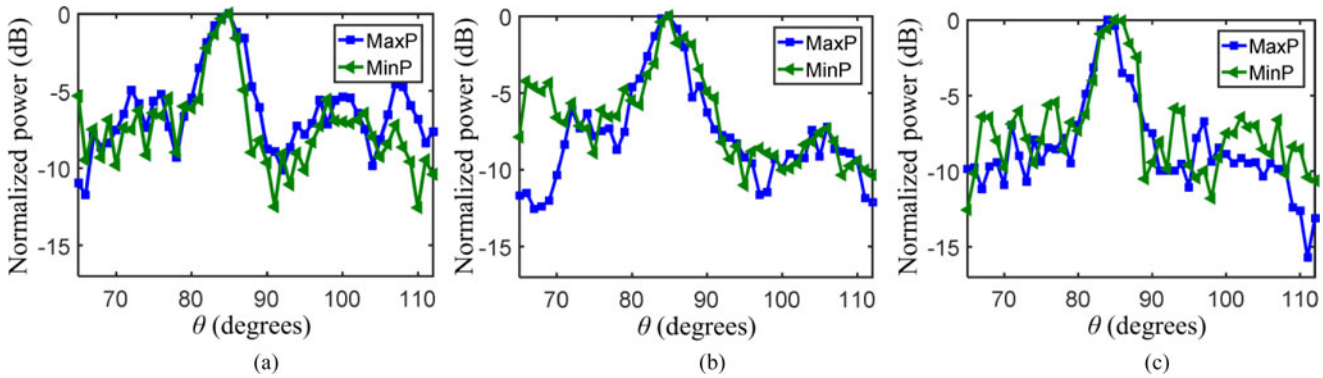

Fig. 5. Normalized measured radiation patterns (in the y-z plane), for two polarization states at the waveguide entrance [TLF stage in Fig. 3(a)] that cause maximum (MaxP) and minimum power (MinP) power reception at the FP with orientation angles (a) $\theta_{f,1} = 85°$, (b) $\theta_{f,2} = 75°$ and (c) $\theta_{f,3} = 65°$. The polarization extinction ratios (the difference between the peak radiation intensities of the MaxP and MinP states) for (a), (b) and (c) are 7.4 dB, 11.37 dB, and 10.52 dB, respectively.

dependence of the measured far-field pattern on the polarization of the wave launched at the TLF [Fig. 3(a)]. Due to the experimental limitations, we can use only the measured far-field signature to identify the polarization of the mode in the OLWA. We carry out two sets of far-field pattern measurements corresponding to two *extreme* states of the polarizations: (i) first the polarization of the launched field is varied via the polarization controller [Fig. 3(a)] to maximize the power reception at the reference angle $\theta_{f,1} = 85°$ and then the radiation pattern is measured as explained in Section III-B without altering this polarization state, namely MaxP state; (ii) again at the same reference angle $\theta_{f,1} = 85°$, the polarization of the wave at the TLF is varied to minimize the power reception and the radiation pattern is measured again for this polarization state, namely MinP state. We then repeat steps (i) and (ii) starting with two other reference angles $\theta_{f,2} = 75°$ and $\theta_{f,3} = 65°$. The motivation of using multiple reference angles arises from the fact that the TM mode may radiate more power than the TE mode at one radiation angle, but it may have less power than TE mode radiation at another angle, as illustrated in Fig. 4. This is also the reason that the polarization state should be tuned at first and then stay intact while sweeping the angle. By changing the reference angle, the polarization state corresponding to MaxP and MinP will change, so that we catch the far-field signature of distinct waveguide modes that may radiate.

Fig. 5 shows the normalized radiation patterns measured in the MaxP and MinP polarization states with respect to the reference angles $\theta_{f,1} = 85°$, $\theta_{f,2} = 75°$, and $\theta_{f,3} = 65°$. The polarization extinction ratios (difference between the peak radiation intensities of MaxP and the MinP states) are 7.4 dB, 11.37 dB and 10.52 dB, respectively, for $\theta_{f,1} = 85°$, $\theta_{f,2} = 75°$, and $\theta_{f,3} = 65°$. The limited extinction ratio may arise from the imperfect polarization control. Theoretically, the OLWA supports both the TE and TM modes and one would expect to observe the different far-field patterns pertaining to the TM and TE input waves among these six radiation patterns in Fig. 5. However, the manipulation of the wave polarization at the TLF stage does not alter the far-field patterns as observed in Fig. 5. The TE mode radiation pattern is expected to be different from the TM mode's, yet none of the polarization states in the 6 cases showed a different far-field signature. This supports the claim that the TM mode's radiation pattern, which is in agreement with the simulated radiation pattern, is detectable, whereas the TE mode suffers from waveguide loss and low radiation directivity in the measured angular range.

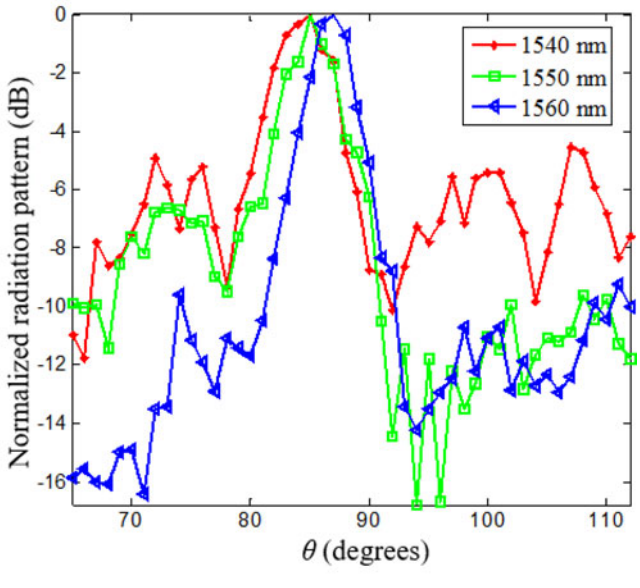

Fig. 6. Measured normalized radiation patterns at wavelengths 1540 nm, 1550 nm and 1560 nm.

The frequency dependence of the measured radiation pattern is reported in Fig. 6 for wavelengths of 1540 nm, 1550 nm and 1560 nm. The radiation pattern at each reported wavelength exhibits a single dominant peak in the angle range between 65° to 112°. The peak locations and half power beam widths of wavelengths 1540 nm, 1550 nm, and 1560 nm are summarized in the Table I. As wavelength increases, the radiation peak angle slightly increases, moving closer to broadside. This is in agreement with the expectations since the leaky-wave mode index in the OLWA slightly decreases as the wavelength decreases.

TABLE I
RADIATION PEAK ANGLES AND HALF-POWER BEAM WIDTHS AT THREE OPERATING WSAVELENGTHS

Wavelength (nm)	Peak angle θ_p (°)	–3 dB beam width (°)
1540	84.4	6.2
1550	85.1	5.0
1560	86.8	4.6

IV. CONCLUSION

We have fabricated an OLWA on a silicon nitride on silicon-on-insulator platform. The quasi far-field radiation pattern of the OLWA has been experimentally characterized in the waveguide symmetry plane, i.e., the *y*-*z* plane. The OLWA has a single directive radiation peak at the angle 85.1° in the range from 65° to 112° at the wavelength of 1550 nm. The side lobe level is at least 7 dB lower than the main peak. The peak radiation angle scans with frequency as expected from a LW antenna and confirmed experimentally. The selection of the input field polarization significantly modifies the measured radiation intensity, but not the radiation pattern, indicating only one propagation mode (the TM one) is successfully turned into a leaky mode. The reason can attribute to the extra loss on the TE mode mainly introduced by fabrication imperfections.

The device can find promising applications in optical communications, especially for multi-wavelength space division applications owing to its capability of beam scanning with frequency, e.g. launching different wavelengths to multi-core fibers. However, this device may also suffer from limited bandwidth in wavelength–division multiplexing applications, because the radiation angle scans with wavelength of operation, and thus the reception location varies as the wavelength changes. As for radiation beam modulation, the Si nanowires can be utilized for optical and electronic modulation. Our earlier work proposed using doped Si wires to form *p*-*n* junctions embedded inside the Si_3N_4 waveguide. The refractive indices around the *p*-*n* junction regions can be altered by carrier plasma effect, thus changing the radiation intensity at a specific angle as previously shown theoretically in [21], [22].

APPENDIX
COMPARISON OF THE RADIATION PATTERN IN THE FRESNEL REGION AND THE FAR-FIELD REGION

In order to assess the validity of radiation pattern measurement in the radiative Fresnel region, here we compare analytically calculated radiation pattern in the ideal far-field (where the distance from antenna tends to infinity) and at a distance in the Fresnel region as in the experiment reported in this article. The radiation excited from the TM mode (electric field polarized in the *y*-*z* plane, which has perfect magnetic conductor symmetry with respect to the *y*-*z* symmetry plane) can be approximately modeled as the radiation from periodically located magnetic dipoles with the period $d = 1000$ nm. In other words we can imagine to apply the equivalence theorem [38] with both electric and magnetic currents and then apply a perfect electric conductor underneath, on the *x*-*z* plane, resulting in only magnetic currents radiating. The excitation phase and amplitude of such magnetic dipoles located at $\mathbf{r}_n = (nd - z_0)\hat{\mathbf{z}}$ is assumed to be determined by the leaky-wave mode wavenumber, $k_{z,-1} = \beta_{z,-1} + i\alpha_z$, as $\mathbf{m}_n = \hat{\mathbf{x}}\exp[ik_{z,-1}(nd - z_0)]$. We consider the OLWA to be 50 magnetic dipoles, $n = 1, \ldots, 50$, each representing radiation from a unit cell of the OLWA in Fig. 1 The electric field's exact and far-field expressions are found as.

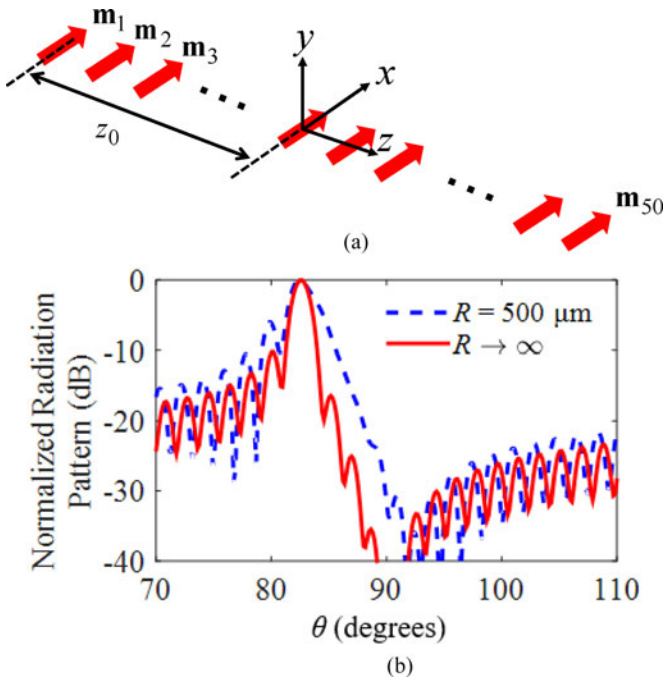

Fig. 7. (a) The antenna array utilized in synthesis of the radiation. (b) The radiation patterns on a constant radius 500 μm and at the far field.

$$\mathbf{E}(\mathbf{R}) = \frac{-\mu_0\omega k}{4\pi}\sum_{n=1}^{50}\frac{e^{ik|\mathbf{R}-\mathbf{r}_n|}}{|\mathbf{R}-\mathbf{r}_n|} \times\left(1+\frac{i}{k|\mathbf{R}-\mathbf{r}_n|}\right)\frac{(\mathbf{R}-\mathbf{r}_n)\times\mathbf{m}_n}{|\mathbf{R}-\mathbf{r}_n|} \quad (A.1)$$

$$\mathbf{E}_{FF}(\mathbf{R}) = \hat{\theta}\frac{e^{ikR}}{R}\frac{-\mu_0\omega k}{4\pi}e^{i(k_{z,-1}-k\cos\theta)\left(\frac{N+1}{2}d-z_0\right)} \times\frac{\sin\left[(k_{z,-1}-k\cos\theta)\frac{Nd}{2}\right]}{\sin\left[(k_{z,-1}-k\cos\theta)\frac{d}{2}\right]} \quad (A.2)$$

where the observation position is $\mathbf{R} = R(\sin\theta\hat{\mathbf{y}} + \cos\theta\hat{\mathbf{z}})$ with R the distance to origin and θ the observation angle. The radiation pattern in the far field region is evaluated as $R|\mathbf{E}_{FF}(\mathbf{R})|$ whereas the one in the Fresnel region is evaluated as $R|\mathbf{E}(\mathbf{R})|$. The latter one depends on the chosen value of R and on the location of the origin of the reference system.

The following results are obtained by assuming the LW wavenumber to be equal to $k_{z,-1} = k_0(0.13 + i0.43 \times 10^{-2})$ at 1550 nm, extracted from full-wave simulations of the OLWA in Fig. 1, carried out by the finite elements method. We also choose $z_0 = 20d$, so that the origin $z = 0$ is located somewhere in the middle of the OLWA, that for $R = 500$ μm it provides the radiation maximum at the same direction as the one of the

far field pattern. Note that this R is comparable to $H = 510\ \mu$m, that is the distance from the OLWA described in Fig. 3.

The synthesized radiation pattern in the y-z plane evaluated from Eq. (A.1) and (A.2) is plotted in Fig. 7(b) versus observation angle θ. It is observed that the Fresnel region pattern correctly recovers the radiation peak at the cost of an increased side-lobe level. This method assures that the measurement in the Fresnel zone described in the body of this paper is able to characterize the main beam also in far field.

REFERENCES

[1] D. R. Jackson and A. A. Oliner, "Leaky-wave antennas," in *Modern Antenna Handbook*, vol. 1. Hoboken, NJ, USA: Wiley, 2008, pp. 325–367.

[2] W. W. Hansen, "Radiating electromagnetic wave guide," U.S. 2 402 622 A, June 25, 1946.

[3] A. A. Oliner, "Leaky-wave antennas," in *Antenna Engineering Handbook*, R. C. Hohnson, Ed. New York, NY, USA: McGraw Hill, 1993.

[4] A. Andreone, "Linear and planar periodic arrays of metallic nanospheres: Fabrication, optical properties and applications," in *Photonic Crystals and Metamaterials*. Singapore: World Scientific, 2011.

[5] T. Thio, K. M. Pellerin, R. A. Linke, H. J. Lezec, and T. W. Ebbesen, "Enhanced light transmission through a single subwavelength aperture," *Opt. Lett.*, vol. 26, no. 24, pp. 1972–1974, Dec. 2001.

[6] T. Thio *et al.*, "Giant optical transmission of sub-wavelength apertures: Physics and applications," *Nanotechnology*, vol. 13, no. 3, pp. 429–432, Jun. 2002.

[7] A. Degiron and T. W. Ebbesen, "Analysis of the transmission process through single apertures surrounded by periodic corrugations," *Opt. Express*, vol. 12, no. 16, pp. 3694–3700, 2004.

[8] D. R. Jackson *et al.*, "The fundamental physics of directive beaming at microwave and optical frequencies and the role of leaky waves," *Proc. IEEE*, vol. 99, no. 10, pp. 1780–1805, Oct. 2011.

[9] D. R. Jackson, J. Chen, R. Qiang, F. Capolino, and A. A. Oliner, "The role of leaky plasmon waves in the directive beaming of light through a subwavelength aperture," *Opt. Express*, vol. 16, no. 26, pp. 21271–21281, Dec. 2008.

[10] X.-X. Liu and A. Alù, "Subwavelength leaky-wave optical nanoantennas: Directive radiation from linear arrays of plasmonic nanoparticles," *Phys. Rev. B*, vol. 82, no. 14, Oct. 2010, Art. no. 144305.

[11] S. Campione, S. Steshenko, and F. Capolino, "Complex bound and leaky modes in chains of plasmonic nanospheres," *Opt. Express*, vol. 19, no. 19, pp. 18345–18363, Sep. 2011.

[12] S. Campione and F. Capolino, "Waveguide and radiation applications of modes in linear chains of plasmonic nanospheres," in *Proc. 2013 URSI Int. Symp. Electromagn. Theory*, 2013, pp. 172–175.

[13] F. K. Schwering and S.-T. Peng, "Design of dielectric grating antennas for millimeter-wave applications," *IEEE Trans. Microw. Theory Tech.*, vol. 31, no. 2, pp. 199–209, Feb. 1983.

[14] A. Alphones and M. Tsutsumi, "Leaky wave radiation from a periodically photoexcited semiconductor slab waveguide," *IEEE Trans. Microw. Theory Tech.*, vol. 43, no. 9, pp. 2435–2441, Sep. 1995.

[15] A. Rofougaran and M. Rofougaran, "Method and system for a smart antenna utilizing leaky wave antennas," U.S. 8 432 326 B2, Apr. 30, 2013.

[16] D. J. Richardson, J. M. Fini, and L. E. Nelson, "Space-division multiplexing in optical fibres," *Nature Photonics*, vol. 7, no. 5, pp. 354–362, May 2013.

[17] J. Sakaguchi *et al.*, "305 Tb/s space division multiplexed transmission using homogeneous 19-Core fiber," *J. Lightw. Technol.*, vol. 31, no. 4, pp. 554–562, Feb. 2013.

[18] P. Baues, H. Mahlein, A. Reichelt, and G. Winzer, "Controllable, electro-optical grating coupler," U.S. 4 006 963 A, Feb. 08, 1977.

[19] D. Taillaert *et al.*, "An out-of-plane grating coupler for efficient butt-coupling between compact planar waveguides and single-mode fibers," *IEEE J. Quantum Electron.*, vol. 38, no. 7, pp. 949–955, Jul. 2002.

[20] Q. Song, S. Campione, O. Boyraz, and F. Capolino, "Silicon-based optical leaky wave antenna with narrow beam radiation," *Opt. Express*, vol. 19, no. 9, pp. 8735–8749, Apr. 2011.

[21] S. Campione, C. Guclu, Q. Song, O. Boyraz, and F. Capolino, "An optical leaky wave antenna with Si perturbations inside a resonator for enhanced optical control of the radiation," *Opt. Express*, vol. 20, no. 19, pp. 21305–21317, Sep. 2012.

[22] C. Guclu, S. Campione, O. Boyraz, and F. Capolino, "Theory of a directive optical leaky wave antenna integrated into a resonator and enhancement of radiation control," *J. Lightw. Technol.*, vol. 32, no. 9, pp. 1741–1749, May 2014.

[23] Q. Zhao *et al.*, "Experimental demonstration of directive Si3N4 optical leaky wave antennas with semiconductor perturbations at near infrared frequencies," *Proc. SPIE*, vol. 9365, pp. 93651K–93651K–10, 2015.

[24] Q. Zhao, Y. Huang, C. Guclu, F. Capolino, and O. Boyraz, "Optical leaky wave antenna experiment demonstration and electronic modulation investigation," in *Proc. Conf. Lasers Electro-Optics*, 2015, Paper JTh2A.43.

[25] Q. Zhao, M. Rajaei, and O. Boyraz, "Silicon nitride on silicon-on-insulator: A platform for integration active control over passive components," in *Proc. Conf. Lasers Electro-Optics*, 2016, PaperJW2A.125.

[26] W. D. Sacher, Y. Huang, G.-Q. Lo, and J. K. S. Poon, "Multilayer silicon nitride-on-silicon integrated photonic platforms and devices," *J. Lightw. Technol.*, vol. 33, no. 4, pp. 901–910, Feb. 2015.

[27] M. J. R. Heck, J. F. Bauters, M. L. Davenport, D. T. Spencer, and J. E. Bowers, "Ultra-low loss waveguide platform and its integration with silicon photonics," *Laser Photon. Rev.*, vol. 8, no. 5, pp. 667–686, Sep. 2014.

[28] Y. Huang *et al.*, "Sub-micron silicon nitride waveguide fabrication using conventional optical lithography," *Opt. Express*, vol. 23, no. 5, pp. 6780–6786, Mar. 2015.

[29] Q. Song *et al.*, "Imaging by silicon on insulator waveguides," *Appl. Phys. Lett.*, vol. 94, no. 23, pp. 231101-231101–3, Jun. 2009.

[30] Y. Huang *et al.*, "Wavelength conversion bandwidth enhancement through quasi-phase-matching in a width modulated silicon waveguide," in *Proc. Opt. Fiber Commun. Conf./Nat. Fiber Optic Eng. Conf. 2013*, 2013, Paper JTh2A.33.

[31] R. Soref, "The past, present, and future of silicon photonics," *IEEE J. Sel. Topics Quantum Electron.*, vol. 12, no. 6, pp. 1678–1687, Nov. 2006.

[32] A. Liu *et al.*, "A high-speed silicon optical modulator based on a metal–oxide–semiconductor capacitor," *Nature*, vol. 427, no. 6975, pp. 615–618, Feb. 2004.

[33] A. Liu *et al.*, "High-speed optical modulation based on carrier depletion in a silicon waveguide," *Opt. Express*, vol. 15, no. 2, pp. 660–668, Jan. 2007.

[34] B. O. Seraphin and N. Bottka, "Franz-keldysh effect of the refractive index in semiconductors," *Phys. Rev.*, vol. 139, no. 2A, pp. A560–A565, Jul. 1965.

[35] Y. Wang, A. S. Helmy, and G. V. Eleftheriades, "Ultra-wideband optical leaky-wave slot antennas," *Opt. Express*, vol. 19, no. 13, p. 12392, Jun. 2011.

[36] G. K. Celler and S. Cristoloveanu, "Frontiers of silicon-on-insulator," *J. Appl. Phys.*, vol. 93, no. 9, pp. 4955–4978, May 2003.

[37] C. A. Balanis, "Linear wire antennas," in *Antenna Theory: Analysis and Design*, 3rd ed. Hoboken, NJ, USA: Wiley, 2005, p. 170.

[38] C. A. Balanis, "Aperture antennas," in *Antenna Theory: Analysis and Design*, 3rd ed. Hoboken, NJ, USA: Wiley, 2005, pp. 653–738.

Qiancheng Zhao (S'16) received the B.S. degree in the Department of Optical Engineering, Zhejiang University, Hangzhou, China, in 2012, and the M.S. degree in the Department of Electrical Engineering and Computer Science, University of California, Irvine (UCI), CA, USA, in 2014, where since 2014, he has been working toward the Ph.D. degree.

He is a student member of the Optical Society of America. He received the Broadcom Fellowship at UCI in 2014.

Caner Guclu (S'10) received the B.S. and M.S. degrees in electrical engineering from the Middle East Technical University (METU), Ankara, Turkey, in 2008 and 2010, respectively. Since 2010, he has been working toward the Ph.D. degree at the University of California, Irvine, CA, USA.

From 2008 to 2010, he was a Research and Teaching Assistant with the Department of Electrical and Electronics Engineering, METU. In November 2009, he worked at Centre Tecnologic de Telecomunicacions de Catalunya as a Visiting Researcher for a Short-Term Scientific Mission funded by COST (European Cooperation in Science and Technology) ASSIST. He was a Visiting Scholar at the Center for Integrated Nanotechnologies, Sandia National Laboratories, in Summer 2013. He has published more than ten peer-reviewed journal articles, more than 20 conference papers, and a book chapter. His research interests include reflect array design, optical leaky wave antennas, hyperbolic metamaterials, and characterization and applications of plasmonic metamaterials and nanostructures.

Mr. Guclu was a recipient of Research Fellowship from the Scientific and Technical Research Council of Turkey from 2009 to 2010. He received the Student Travel Fellowship by the Union for Radio Science National Committee for 2013 and 2014.

Yuewang Huang received the B.S. degree in electrical engineering from the Beijing University of Posts and Telecommunications, Beijing, China, in 2009, and the M.S. and Ph.D. degrees in electrical engineering from the University of California, Irvine, CA, USA, in 2010 and 2014, respectively. Since 2014, he has been with Apple Inc., Cupertino, CA, as an RF Engineer. His research interests include sensors, microwave, nonlinear optics, waveguides, metamaterial, and infrared optics.

Filippo Capolino (S'94–M'97–SM'04) received the Laurea (cum laude) and Ph.D. degrees in electrical engineering from the University of Florence, Florence, Italy, in 1993 and 1997, respectively.

He is currently an Associate Professor in the Department of Electrical Engineering and Computer Science, University of California, Irvine, CA, USA. Previously, he was an Assistant Professor in the Department of Information Engineering, University of Siena, Siena, Italy. From 1997 to 1999, he was a Postdoctoral Fellow with the Department of Aerospace and Mechanical Engineering, Boston University, Boston, MA, USA. From 2000 to 2001 and in 2006, he was a Research Assistant Visiting Professor with the Department of Electrical and Computer Engineering, University of Houston, Houston, TX, USA. His research interests include antennas, metamaterials and their applications, sensors in both microwave and optical ranges, wireless systems, chip-integrated antennas. He was the EU Coordinator of the EU Doctoral Programs on Metamaterials from 2004 to 2009.

Dr. Capolino is a member of the Optical Society of America and the International Society for Optical Engineers. He received the R. W. P. King Prize Paper Award from the IEEE Antennas and Propagation Society for the Best Paper of the Year 2000, by an author under 36. From 2002 to 2008, he served as an Associate Editor for the IEEE TRANSACTIONS ON ANTENNAS AND PROPAGATION. He is the Editor of the *Metamaterials Handbook* (Boca Raton, FL, USA: CRC Press, 2009).

Ozdal Boyraz received the B.S. degree in electrical engineering from Hacettepe University, Ankara, Turkey, in 1993, and the M.S. and Ph.D. degrees in electrical engineering from the University of Michigan, Ann Arbor, MI, USA, 1997 and 2001, respectively.

After graduation, he worked as an R&D Engineer at Xtera Communications, Allen, TX, USA, for two years, and as a Postdoctoral Scholar at the University of California, Los Angeles, CA, USA. After completing the postdoctoral study, he joined the Electrical Engineering and Computer Science Departments, University of California, Irvine, CA, as an Assistant Professor in 2005. He currently serves as an Associate Professor in the same department as well as in the Materials Science and Engineering Program. His research areas include silicon-based photonic devices, nonlinear optical devices, optical communication systems, and optical signal processing.

Dr. Boyraz is a member of the Optical Society of America. He is a recipient of 2010 DARPA Young Faculty Award and 2005 IEICE Electronic Express Best Paper Award.